

AD A094398

AFIT/GEP/PH/80D-8

SECRET

II

①

14 JAN 1981

APPROVED FOR PUBLIC RELEASE AFR 190-17.

Fredric C. Lynch

FREDRIC C. LYNCH, Major, USAF
Director of Public Affairs

Air Force Institute of Technology (AFIT)
Wright-Patterson AFB, OH 45433

INVESTIGATION OF ELECTRON LOSS
PROCESSES IN CO₂/He/N₂
ELECTRIC DISCHARGES

THESIS

AFIT/GEP/PH/80D-8

Greg R. Schneider
Capt USAF

Preface

Of all of the results from this study, the most significant to me was the growth of my knowledge of laboratory procedures. Most of the fine points of lab work are not taught in the classroom but must be learned first-hand. Yet it is attention to these same details that often makes the difference between success and failure. I am grateful for the opportunity to gain this lab experience that will prove invaluable to me in the future.

The technical and moral support provided by the members and contractors of the Energy Conversion Branch of the Air Force Aero Propulsion Laboratory was nothing less than outstanding. In particular, Mr. Robert Knight, Mr. D. Clifford Van Sickle, Mr. Ben Sarka, Mr. Dennis Grosjean, and Mr. Walt Balster were of invaluable assistance during the course of this project. My thanks go to Dr. Alan Garscadden for enlightening discussions and rapid response to my equipment requests. Lt. Col. William F. Bailey provided helpful guidance in the preparation of this report. Unquestionably, this project could not have been completed without the preparation, patience, direction, and experience of my adviser, Dr. Peter Bletzinger. Finally, I wish to thank my wife and daughter, without whose support, sacrifice, and work, I never could have begun this project, let alone finish it.

Greg R. Schneider

Contents

	Page
Preface	ii
List of Figures	v
List of Tables	vi
List of Symbols	vii
Abstract	x
I. Introduction	1
Problem	1
Assumptions	1
Approach	2
Sequence of Presentation	2
II. Background	4
Structure of a Discharge	4
Electron Kinetics	7
Plasma Chemistry	14
III. Theory	19
Temporal History of Electrons	19
Considerations of High-Pressure Operation	23
IV. Experimental Apparatus	24
Gas Mixture	24
Electron Gun	26
Discharge Chamber	29
Closed-Cycle Flow Loop	33
Diagnostics and Data Reduction	34
V. Results and Analysis	41
Measurements in CO ₂ Mix	41
Measurements in N ₂	44
Data Modifications	46
Steady-State Analysis	50
VI. Conclusions and Recommendations	55
Bibliography	57

Contents

	Page
Appendix: Error Analysis	59
Cathode Fall	59
Equipment Error	60
Vita	62

List of Figures

<u>Figure</u>		<u>Page</u>
1	Structure of a Glow Discharge	6
2	Experimental Apparatus Schematic	25
3	Flow Loop Leak Rate	31
4	Calculated Current Decay Curves	42
5	Discharge Current Pulse	45
6	Calculated Electron Production Rate vs Steady-State Electron Number Density	51
7	Experimental Electron Production Rate vs Steady-State Electron Number Density	52

List of Tables

<u>Table</u>		<u>Page</u>
I	Electron Kinetic Reactions	11
II	CO ₂ /N ₂ /He Electron Kinetics	15
III	Plasma Chemistry Reactions	17
IV	Nonlinear Curve Fit Results	37
V	Rate Errors vs Number Density Ratio	40
VI	CO ₂ Data	43
VII	N ₂ Data	47
VIII	Measured Rates in N ₂	48
IX	Equipment and Signal Accuracies	60

List of Symbols

A	Collector area (cm^2)
A	Ampere
cm	Centimeter (0.01 meter)
CW	Continuous wave
dE/dm	Mean stopping power of gas ($\text{eV}\cdot\text{cm}^2/\text{g}$)
e	Electronic charge (1.6×10^{-19} Coulomb)
e	Electron
E	Electric field strength (V/cm)
E_i	Effective ionization potential (V)
eV	Electron volt
f	Farad
g	Gram
h	Planck's constant (6.626×10^{-34} Joule-sec)
Hz	Hertz (1 cycle/sec)
I	Current (Amperes)
j	Current density (A/cm^2)
J_{eb}	Electron beam current density (A/cm^2)
k_i	Ion-ion recombination rate (cm^3/sec)
kV	Kilovolt (1000 volts)
kW	Kilowatt (1000 watts)
M	Mean gas molecular weight (g)
mA	Milliampere (0.001 Ampere)
m_p	Mass of proton (1.673×10^{-24} g)
mm	Millimeter (0.001 meter)
N	Neutral gas number density (cm^{-3})

n_a	Number density of attaching species (cm^{-3})
n_e	Number density of electrons (cm^{-3})
n_{e0}	Number density of electron at steady-state (cm^{-3})
n_f	Final number density of electrons (cm^{-3})
n_-	Number density of negative ions (cm^{-3})
n_+	Number density of positive ions (cm^{-3})
s	Electron beam electron-ion pair production rate (sec^{-1})
t	Time (sec)
T	Townsend ($1 \times 10^{-17} \text{ V-cm}^2$)
T_e	Electron temperature (eV)
V	Volt
W_e	Electron drift velocity (cm/sec)
W_-	Negative ion drift velocity (cm/sec)
W_+	Positive ion drift velocity (cm/sec)
z	Townsend ionization coefficient (cm^{-1})
α	Electron-ion recombination rate (cm^3/sec)
β	Inverse attachment time (sec^{-1})
γ	Attachment coefficient (cm^3/sec)
ϵ	$\alpha n_{e0} + (1/2)\beta$
λ_d	Debye length (cm)
μ	Micro (10^{-6})
ν	Frequency (sec^{-1})
σ	Diffusion coefficient (cm^2/sec)
*	Excited species
$^{\circ}\text{C}$	Degrees centigrade

°K Degrees Kelvin
∇ Gradient
- Negative charge
+ Positive charge

Abstract

An investigation of electron loss processes in electron beam-sustained discharges of an atmospheric pressure gas mixture of 1/1.6/3, CO₂/He/N₂ in a closed-cycle flow loop was conducted. Steady-state analysis of the discharge current indicates that the discharge is dominated by electron-neutral attachment at rates of approximately 10^6 sec^{-1} in the E/N range of 0.5-9 Townsend. Attempts to fit an analytic solution of the electron lifetime equation to the discharge current decay curves were inconclusive due to the slow fall-time of the electron gun relative to the current decay time. Changes in the discharge characteristics due to chemical reactions in the plasma were not significant.

INVESTIGATION OF ELECTRON LOSS PROCESSES IN
CO₂/He/N₂ ELECTRIC DISCHARGES

I Introduction

Project Viper at the Air Force Weapons Laboratory calls for the construction of a large scale, pulsed, electron beam-sustained CO₂ laser to be used to perform studies of the effects of laser radiation on various materials. The design of the laser requires accurate prediction of its performance. Such predictions are based on a detailed knowledge of the behavior of the discharge plasma. The following work sought to contribute to that knowledge.

Problem

The objective of this experiment was to determine electron loss rates in an atmospheric pressure mixture of 1/1.6/3, CO₂/He/N₂ in a closed-cycle, electron beam-sustained discharge.

Assumptions

The major assumptions noted here are discussed in more detail in later sections. Electron diffusion losses were assumed to be negligible due to the large size of the discharge chamber and operation at atmospheric pressure. The plasma was assumed to be electrically neutral, i.e., the number of electrons and negative ions equals the number of positive ions present. The electric field across the discharge was assumed to be uniform and constant.

Approach

The fundamental guideline was to, within the confines of available equipment, replicate the proposed operating conditions of the Viper device with respect to gas mixture, pressure, and electric field. The basic procedure was to analyze the decay of the discharge current after the termination of external ionization. A pulsed electron beam-sustained discharge, to be described in more detail later, was formed in a quartz-lined stainless steel chamber within a closed-cycle gas flow loop. The current decay was to be recorded by a high-speed digitizer having a resolution greater than that of a standard oscilloscope. The plot of the current decay from the digitizer was to be digitized by a computer and a non-linear least-squares fit to the data performed. By varying the voltage across the discharge and/or the current from the electron beam, measurements can be obtained for a variety of electrical conditions. In addition, analysis of the relationship of the steady-state current to the ionization source strength was performed.

Sequence of Presentation

First, a general background discussion of the important discharge characteristics including structure, electron formation and loss processes, and chemical reactions within the plasma will be presented. Next, the general mathematical description of the plasma will be discussed with a greater emphasis on the specific theory appropriate for this experiment. Third, a discussion of the experimental apparatus

and methods will point out the unique characteristics of this experiment as well as some of the problems encountered during the course of the project. Fourth, the results obtained will be analyzed in light of results of other authors and with respect to theoretical predictions. Finally, conclusions and recommendations about the results, apparatus, and procedures will be presented.

II Background

A gas discharge is the conduction of electricity through a gaseous medium. A discharge may be very short in duration as in a spark or lightning strike, or continue for hours as with a neon light. As most gases are insulators under normal conditions, certain fundamental changes in composition must take place to change the gas to a conductor. This section discusses those changes in general and for the specific gas mix and experimental set-up used in this study.

Structure of a Discharge

Most gases at room temperature, atmospheric pressure, and under no external influences are electrically neutral containing few free electrons and ions. The few electrons and ions present are a result of ionization by natural processes such as cosmic rays. To conduct electricity efficiently, the gas must acquire more charge carriers either from an external source and/or from ionization of the gas molecules. As the number of charge carriers increases, the gas changes to a plasma. One criteria for differentiating a plasma from a normal gas is that the distance within which internal or external electrostatic fields are shielded, called a Debye length, be much smaller than the characteristic dimension of the vessel containing the plasma. The Debye length, λ_d , of a plasma having an electron number

density of n_e per cm^3 at an electron temperature of T_e can be calculated from

$$\lambda_d = 6.9(T_e/n_e)^{\frac{1}{2}} \quad (\text{Ref 3:4}) \quad (1)$$

Another plasma criterion is that the number of electrons within a sphere of radius equal to the Debye length be much greater than one. For the conditions of this experiment, n_e was 10^9 - 10^{12} per cm^3 and T_e was approximately $11,600^\circ\text{K}$ (1 eV), so λ_d was 7.4×10^{-4} cm to 2.35×10^{-2} cm. Further, the number of electrons within a Debye sphere ranged from about 1.7×10^3 to 5.4×10^4 . These results meet the above criteria. Since the Debye length was smaller than the chamber dimensions and beyond a Debye length the plasma is electrically neutral, the plasma was assumed to be electrically neutral throughout the discharge region.

There are different kinds of discharges each having different characteristics. Of interest here was the glow discharge which has shown itself to be an efficient laser medium. The glow discharge is so called because of the luminosity of the positive column. Figure 1 is a generic diagram of a glow discharge. It will be noted that the positive column occupies the majority of the space between the electrodes. In the positive column, the electric field, charge density, and current density are virtually constant in the axial direction so that a relatively homogeneous medium is formed. Under certain conditions, however, the positive column can become striated with light and dark

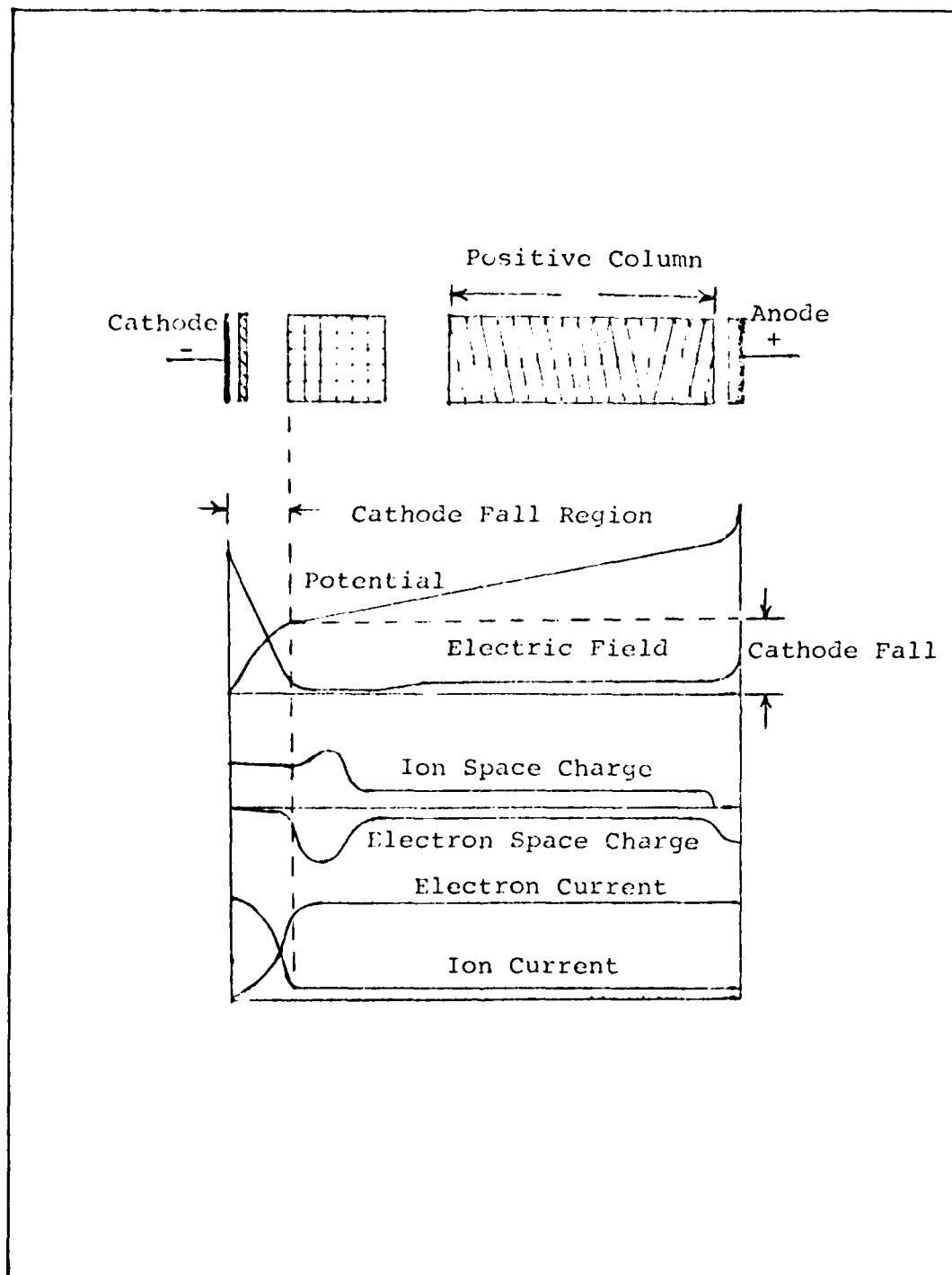


Fig 1. Structure of a Glow Discharge (Ref 20:218)

regions such that the properties of the column are oscillatory with respect to axial distance.

The regions near the cathode are typically very small axially and play only minor roles in the processes to be studied here. The cathode fall region is a portion of the discharge over which a significant drop in potential occurs. This potential drop typically reduces the effective potential across the positive column by a few hundred volts and should be accounted for when analyzing the electrical characteristics of the positive column. The cathode fall results from the presence of very large fields (orders of magnitude greater than those in the positive column) due to a high concentration of ions. Such fields are necessary for the emission of electrons by the cathode. The region is of small extent because of the limited range over which the high fields exist. Since the cathode regions are small and the cathode fall can be experimentally dealt with, the assumption of a uniform field across the discharge is a good one.

Electron Kinetics

The formation of a plasma as mentioned above requires a reasonably large number of charged particles, ions and electrons, to be introduced in the medium either from an external source and/or from ionization of the medium itself. This section will discuss the processes by which these charged particles are produced and lost in a discharge.

The current density carried by a plasma can be calculated from

$$j = (n_e W_e + n_+ W_+ + n_- W_-) e \quad (\text{Ref 6:10}) \quad (2)$$

where

j = current density (amps/cm²)

n_e, n_+, n_- = number density of electrons, positive and negative ions, respectively (cm⁻³)

W_e, W_+, W_- = drift velocities of electrons, positive and negative ions, respectively (cm/sec)

e = electronic charge (1.6×10^{-19} Coulomb)

But, since the force on each electron or ion is the same, the relative drift velocities are proportional to the ratio of the masses of the particles. The drift velocity is also inversely proportional to the collision frequency of the species. The electron-neutral collision frequency is lower than that for ion-neutral collisions. Thus, W_e is much greater than W_+ or W_- , so that most of the current is carried by the electrons. For this reason, this report will primarily deal with electron gain and loss processes and only consider the ions as they pertain to those processes.

Ionization. There are two types of glow discharges differentiated by the source of ionization. In the self-sustained discharge, a high electric field is established across the plasma by placing a high voltage between the electrodes. The field is large enough to impart enough

energy to the free electrons so that they will ionize the neutral gas at a rate at least equal to the electron loss rate. The discharge is called self-sustained because it produces its own ionization and requires no auxiliary ionization source.

The second type of discharge, the non-self-sustained discharge, uses some external source of electrons to provide ionization. External sources of electrons commonly are heated cathodes and electron guns. The present system utilizes the latter which fires a stream of high-energy electrons through a thin metal foil into the gas mixture. The high-energy primary electrons ionize the gas producing many low-energy secondary electrons. Thus, a high background electron number density is established. The energy of these secondary electrons is tailored by the sustainer field.

An electron within the plasma is accelerated by the sustainer field and collides with other electrons, ions, and neutral species. If the electron transfers enough energy to the neutral species, that species can be ionized yielding a positive ion and another electron. If the energy transferred is not sufficient for ionization, it may still be enough to excite the species to a state of higher energy. These excited state molecules can then be subsequently ionized by electron collision or collision with another excited state molecule. The excited state molecules may decay through collisions with lower state molecules or by

emission of photons. This latter case is the source of the light from a glow discharge and for a laser. Table I lists these reactions for generic species A and B.

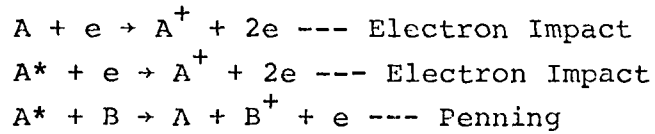
The amount of ionization taking place depends on the electron energy distribution, the ionization potential of the particular molecule, and the probability of a collision between the molecule and an electron having energy equal to or greater than the ionization potential. The latter two parameters are essentially fixed as they are species dependent. The electron energy distribution, which tells how many electrons are at each energy, can be changed by controlling the ratio of the electric field strength to the neutral number density of the gas (E/N). By changing the electrode separation or the voltage between them, the field can be varied. The gas number density is easily varied by changing the pressure at constant temperature. In a non-self-sustained discharge, the E/N is low so that there is insufficient ionization by secondary electrons to maintain the discharge after removal of the external ionization source. For self-sustained discharges, the opposite is true and the plasma will continue as long as voltage is applied to the electrodes. A common example of the latter case is a fluorescent light. In the present case, the plasma only exists, or is sustained, when the electron gun is operating.

Diffusion. All electric discharges will extinguish when the ionization rate falls below the electron loss rate. One process by which electrons are removed from the discharge

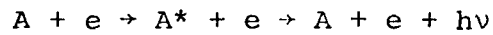
TABLE I

Electron Kinetic Reactions

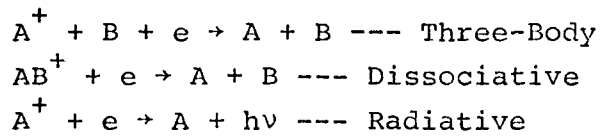
Ionization



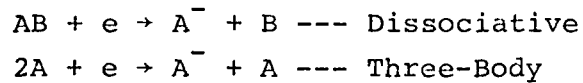
Excitation



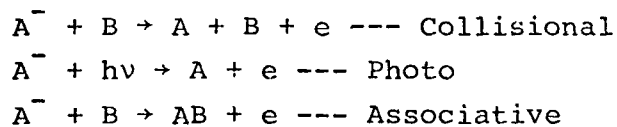
Recombination



Attachment



Detachment



is diffusion. As the electrons move through the plasma, collisions cause them to travel fairly random paths. In so doing, some electrons collide with the walls of the chamber and are removed from the discharge. Thus, there are fewer electrons near the walls than in the center of the plasma and a gradient in the electron number density is established. Similar to normal gas diffusion motion, the electrons will tend to move from the high concentration area in the plasma core to the lower concentration areas near the walls. The diffusion time is proportional to the neutral molecule number density and the square of the distance to the wall. Thus, the higher the pressure and/or the larger the chamber, the longer the diffusion time. This reduces the diffusion loss for large-scale, high pressure systems.

Recombination. As the name implies, recombination is essentially the joining of a free electron and a positive ion to re-form a neutral particle. The rate of recombination depends on the numbers of electrons and positive ions present. Since, as noted above, the number of positive ions is approximately equal to the number of electrons, recombination is essentially a function of the square of the electron number density. As with ionization, the electron energy distribution and the necessary collision cross-section determine a rate coefficient dependent on E/N . The actual process of recombination in glow discharges usually has three forms as denoted in Table I. Since recombination releases energy, each method requires some way to remove

this energy. In three-body recombination, a third particle, usually a neutral species, carries off the excess energy as kinetic energy. Dissociative recombination dissipates the energy by yielding two neutral species with additional kinetic energy. Finally, radiative recombination yields the excess energy as a photon. Recombination is the primary electron loss mechanism in ideal high pressure glow discharges. It is this rate that this study attempted to determine.

Attachment. The third electron loss process is electron-neutral attachment, in which a free electron and a neutral species combine to form a negative ion. Only a relatively few species exhibit significant attachment rates. Some of these species are O_2 , O , and CO_2 . While attachment should be a less prominent process than recombination in this experiment, it cannot be neglected because of the presence of CO_2 and the possibility of forming O_2 , O , and other attaching species through plasma chemical reactions.

Attachment usually has two forms as shown in Table I. In dissociative attachment, the neutral species breaks up with one of the pieces becoming the negative ion. Three-body attachment occurs less frequently and is analogous to three-body recombination. The attachment rate, as the others, is dependent on the number of electrons present and their energy distribution. The rate is also dependent on the number density of the attaching species and the associated cross-section.

Detachment. The final process to be discussed is detachment, which is essentially the inverse of attachment. The collisional detachment process shown in Table I stems from the collision of a neutral species and a negative ion yielding two neutral particles and an electron. For this experiment the detachment rate will not be considered explicitly. Rather, the attachment rate considered will be a net rate encompassing both attachment and detachment.

Wiegand and Nighan have analyzed the electron kinetics in $\text{CO}_2/\text{N}_2/\text{He}$ discharges (Ref 21:583). Table II lists the reactions they consider to be dominant. While their studies were for pressures up to 100 Torr, operation at atmospheric pressure should not change the list of relevant processes since ionization and attachment scale with pressure and recombination is independent of pressure (Ref 11:287). Further, Bletzinger et. al. have investigated contaminants in $\text{CO}_2/\text{N}_2/\text{He}$ discharges to determine their effects (Ref 2:317-323). Table II also lists some of the reactions they found to be possibly important.

Plasma Chemistry

In order to understand what is happening in a given discharge, one needs to know what species are present. This is done most often with a mass spectrometer. Other methods include using tunable lasers to measure absorption or gain at known energy levels of the particular species under study. Due to time and equipment constraints, none of

TABLE II
CO₂/N₂/He Electron Kinetics

<u>Ionization</u>	<u>Rate Coefficient (cm³sec⁻¹)</u>	<u>Ref</u>
CO ₂ + e → CO ₂ ⁺ + 2e	1x10 ⁻¹⁴ - 2x10 ⁻¹²	21:583
N ₂ [*] + e → N ₂ ⁺ + 2e	1x10 ⁻¹¹ - 1x10 ⁻⁹	21:583
<u>Recombination</u>		
O ₂ ⁺ + e → 2O	2x10 ⁻⁸	21:583
O ⁻ + O ₂ ⁺ → O + O ₂	1x10 ⁻⁷	21:583
<u>Attachment</u>		
CO ₂ + e → CO + O ⁻	3x10 ⁻¹³ - 2x10 ⁻¹²	21:583
O ₂ + e → O + O ⁻	1x10 ⁻¹²	2:320
<u>Detachment</u>		
CO + O ⁻ → CO ₂ + e	5x10 ⁻¹⁰	21:583
NO + O ⁻ → NO ₂ + e	2.5x10 ⁻¹⁰	19:15

these methods were employed for this experiment. Determining the exact species present or exact process taking place was beyond the scope of this study. Yet, for a better understanding, a brief discussion of the plasma chemistry processes at work in $\text{CO}_2/\text{He}/\text{N}_2$ discharges is warranted.

The plasma chemistry of N_2 and $\text{CO}_2/\text{N}_2/\text{He}$ discharges has been studied by a variety of authors. This section will summarize some of the important aspects of these studies as they relate to the present experiment. Tannen, et. al. observed the formation of O_2 , NO , NO_2 , and CO with the oxygen being generated by dissociation of the CO_2 (Ref 18:7). He also noted the presence of NO^+ , O_2^+ , CO_2^+ , N_2^+ , and CO^+ , all of which can contribute to the recombination rate of the mixture (Ref 18:9). While most of Tannen's measurements were done at less than 10 torr, some of the observed species should be created at high pressure also. Kasner and Biondi have observed that at higher pressures N_4^+ becomes the dominant ion and thus should be considered for the present test (Ref 12:317). Eckbreth and Blaszkus have operated closed-cycle $\text{CO}_2/\text{N}_2/\text{He}$ discharges in the 20-40 torr range and have observed the formation of the same neutral species as Tannen with the exception of NO_2 (Ref 7:4). Wiegand and Nighan developed a computer model of the plasma chemistry inside $\text{CO}_2/\text{He}/\text{N}_2$ discharges which considers about 300 reactions (Ref 21). Their predictions show the accumulation of the same neutral species observed by Tannen and Eckbreth, as well as ions such as CO_3^- , CO_4^- , NO_3^- , and NO_2^- .

The formation of such ions indicates that attachment may be more predominant than just that expected from O_2 . Thoenes and Kurzius have developed a computer model for closed-cycle, electron beam-sustained lasers that predicts not only laser performance but also species formation based upon a large number of reactions both electron kinetic and chemical (Ref 19:11-26). Table III lists some of the chemical reactions considered which might be important to this experiment.

TABLE III

Plasma Chemistry Reactions

<u>Reaction</u>
$CO_2 + e \rightarrow O^- + CO$
$NO_2 + e \rightarrow O^- + NO$
$O^- + CO \rightarrow CO_2^* + e$
$CO_2^+ + e \rightarrow CO + O$
$CO_2^+ + O_2^- \rightarrow CO + O_2 + O$
$CO_2^+ + CO_3^- \rightarrow 2CO_2^* + O$
$N_2^* + CO_2 \rightarrow N + NO + CO$
$O_2^- + N \rightarrow e + NO_2$
$CO_2^+ + NO_2^- \rightarrow CO^* + O + NO_2$

The concern over the formation of these contaminant species stems from the desire to operate this kind of laser in a closed-cycle configuration. Ideally, a lasing species excited as described above will return to its original state upon release of the excitation energy. Thus, the

same molecule or set of molecules can be used repeatedly to produce laser radiation. In reality, however, Bletzinger, et. al. found that small amounts of NO, CO, etc. seriously degrade the performance of the laser (Ref 2). Further, Eckbreth and Blaszyk have found that indeed these species are created and remain in such a closed-cycle system (Ref 7). As the present experiment is performed in a closed-cycle loop, the opportunity to observe the effects, if any, of these contaminants will be exercised by looking for significant changes in discharge performance as a function of time. It should be understood, however, that even if a contaminant does not degrade the discharge performance, it could hamper the lasing process by quenching the excited state or absorbing the emitted radiation. Conversely, a species that does degrade the discharge performance may have no effect on the lasing performance. Thus, any plasma chemical results based on the present analysis will be inconclusive as to the overall effect on laser output.

III Theory

Analysis of the experimental data required a theoretical model of the discharge processes. This section develops the relevant equations and considerations necessary for such analysis.

Temporal History of Electrons

The change in the number densities of the electrons and positive and negative ions with respect to time can be expressed as

$$\frac{dn_e}{dt} = s - \alpha n_e n_+ - \beta n_e - \sigma \nabla^2 n_e + z n_e N \quad (3)$$

$$\frac{dn_+}{dt} = s + z n_e N - \alpha n_e n_+ - k_i n_+ n_- \quad (4)$$

$$\frac{dn_-}{dt} = \beta n_e - k_i n_+ n_- \quad (\text{Ref } 6:10;4:4821) \quad (5)$$

where

n_e, n_+, n_- = number density of electrons, positive and negative ions, respectively (cm^{-3})

t = time (sec)

s = electron beam electron-ion pair production rate (sec^{-1})

α = electron-ion recombination rate (cm^3/sec)

β = inverse attachment time or net attachment rate (sec^{-1}) ($\beta = \gamma n_a$, where γ is the attachment coefficient and n_a is the number density of the attaching species)

σ = diffusion coefficient (cm^2/sec)

z = Townsend ionization coefficient (cm^{-1})

N = neutral gas number density (cm^{-3})

k_i = ion-ion recombination rate

Collectively, the above equations describe the growth and decay of all of the charged particles in the discharge. However, as mentioned above, the relative drift velocities of the particles result in the bulk of the discharge current being carried by the electrons. Further, the ionization and excitation taking place within the plasma are due primarily to electron-neutral collisions. For these reasons, it is the rise and fall of the electron number density that predominantly determines plasma performance. Thus, Eq. (3) shall be used to describe the present experiment. On a more practical level, the electron number density can be calculated from the discharge current by

$$n_e = I / (A_e W_e) \quad (6)$$

where

I = discharge current (Amps)

A = area of the current collector (cm^2)

Calculation of W_e was accomplished using a numerical solution to the Boltzmann equation for the gas mix in question (Ref 9).

As discussed previously, for the large chamber size and high pressure used in this experiment, the diffusion

time is much greater than that of recombination or attachment so that the diffusion term in Eq. (3) can be neglected. Phelps and Hake have calculated that the average energy of the secondary electrons liberated through ionization by the primary electron beam electrons is so low that ionization by these secondary electrons is not significant in the E/N range of 1-20 Townsend of this experiment (Ref 15:81). This fact is further substantiated by the fact that the discharge is not self-sustained and decays immediately upon removal of the electron beam ionization source. Thus, the Townsend ionization term can be neglected from Eq. (3). The resulting equation

$$\frac{dn_e}{dt} = s - \alpha n_e^2 - \beta n_e \quad (7)$$

(where the assumption of electrical neutrality has been applied to the recombination term) can be integrated with $t = 0$ at ionization turn-on to yield

$$n_e/n_{e0} = \tanhct[(\alpha n_{e0} + \beta)(e^{2\epsilon t} + 1)/((\alpha n_{e0} + \beta)(e^{2\epsilon t} + 1) - \beta)] \quad (8)$$

where

$$\epsilon = \alpha n_{e0} + \beta/2 \quad (\text{Ref 4:4822}) \quad (9)$$

n_{e0} = steady state electron number density (cm^{-3})

From Eq. (7) it is seen that at steady state

$$s = \alpha n_e^2 + \beta n_e \quad (10)$$

Further s can be calculated from

$$s = J_{eb} (NMm_p/eE_i) (dE/dm) \quad (\text{Ref 4:4822}) \quad (11)$$

where

J_{eb} = electron beam current density (A/cm^2)

M = mean gas molecular weight (g)

m_p = mass of a proton (g)

E_i = effective ionization potential (volts)

dE/dm = mean stopping power of gas ($eV \cdot cm^2/g$)

Use of Eqs. (8-11) would allow calculation of the recombination and attachment coefficients by examining the rise in the discharge current. An alternative method using the fall of the discharge current after termination of ionization can also be used.

If Eq. (7) is integrated from the termination of ionization with $t = 0$ and $n = n_{eo}$ at that point then

$$n_e = n_{eo} / ((\alpha n_{eo} / \beta + 1) e^{\beta t} - (\alpha n_{eo} / \beta)) \quad (12)$$

For the case where attachment is negligible, Eq. (7) can be integrated to yield

$$n_e = n_{eo} / (1 + \alpha n_{eo} t) \quad (13)$$

Use of Eq. (12) does not require any calculation of s and is a simpler equation than Eq. (8). Further, since the current decay time is usually much longer than the rise time, it is experimentally easier to monitor the current decay.

Considerations of High-Pressure Operation

As noted previously, ionization and attachment scale directly with pressure while the recombination coefficient is independent of pressure. However, while the recombination coefficient is independent of pressure, the process scales as the square of the electron number density which, in turn, scales with ionization. Thus, it is not clear how the relative magnitudes of the attachment and recombination processes will be affected by high pressure operation.

IV Experimental Apparatus

The Viper device to be built by the Air Force Weapons Laboratory will be a large-scale, electron beam-sustained discharge laser utilizing an open-cycle flow configuration. The device used in this experiment was somewhat similar except that it was closed-cycle. This section will discuss the equipment used as shown schematically in Figure 2, some of the rationale for its use, procedures followed, and some of the problems encountered with this particular set-up.

Gas Mixture

It is proposed that the Viper laser operate without material windows separating the discharge from the atmosphere. This is desirable since there is no known material transparent enough at the 10.6 μm wavelength of the laser that it would not fracture under the high heat loads and photon fluxes it would be exposed to in this device. Windowless operation requires that some other provision be made to keep the plasma from being contaminated by the atmosphere. Most simply this can be accomplished by maintaining a positive pressure gradient inside the chamber so that gas only flows out of the window. Thus, the Viper discharge will be operated at or near atmospheric pressure.

The particular gas mixture of 1/1.6/3, $\text{CO}_2/\text{He}/\text{N}_2$ was chosen because its refractive index most closely approximates that of the atmosphere at the laser site. This index matching is important to prevent the beam from bending or

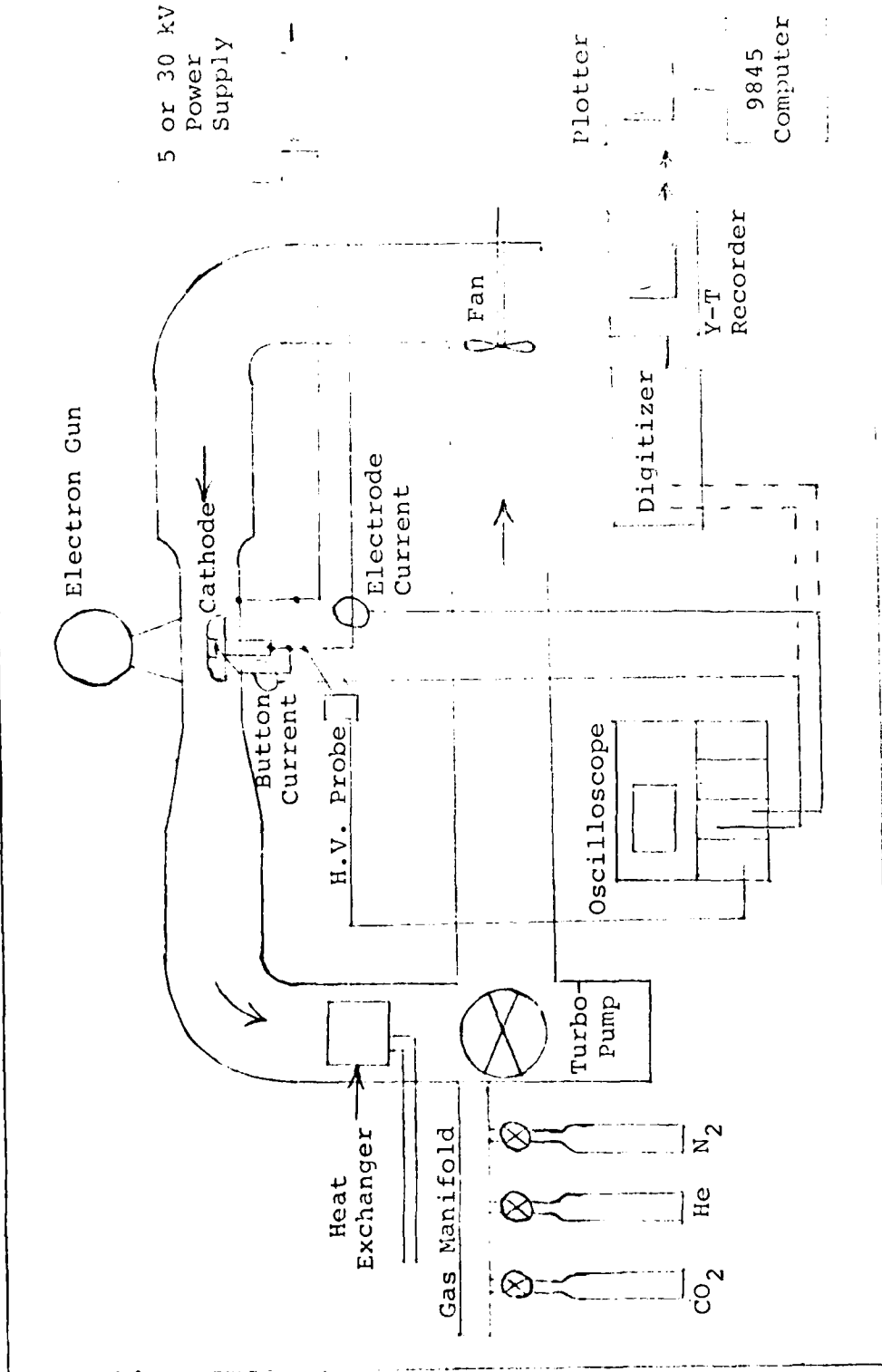


Fig 2. Experimental Apparatus Schematic

refracting at the window due to a change in the index of refraction. These considerations dictated the gas mixture and pressure for this experiment.

Electron Gun

Early designs of electric discharge lasers called for the ionization of the gas to be produced by placing very high potentials across the electrodes causing the formation of a self-sustained discharge. While simple in design, the systems had serious problems with the discharge collapsing to an arc at high pressures due to electron avalanche. Pressure scaling was necessary for higher output power but, to prevent arc formation, the discharges could only be operated for microsecond or less time scales, which restricted the amount of energy deposited. Work by Reilly and Fenstermacher, et. al., demonstrated an alternative method whereby the ionization source was separated from the energy deposition source (Ref 16,8). The technique was to use an electron gun to deposit primary electrons which would ionize the gas, creating the plasma. An electric field, called the sustainer field, is generated across the plasma by placing a potential difference (voltage) between the electrodes. The applied voltage provides the electrons with the proper amount of energy to excite the molecules to the proper level but is low enough so that additional ionization is negligible (Ref 16:3411-3412). Since the plasma exists only as long as the electron gun is on and supplying

ionization, the discharge is said to be electron beam-sustained. Such a system provides two controls on the plasma and yields stable high pressure discharges which are scalable to large volumes. Kast and Cason have shown that electron beam-controlled lasers hold more promise for scaling and efficiency than the pulsed, self-sustained type (Ref 13).

Electron beam-sustained lasers can be operated either pulsed or continuous wave (CW). The Viper device will be a pulsed system to allow more detailed investigation of the laser-target interaction of pulsed lasers.

The device used for this experiment is, likewise, a pulsed, electron beam-sustained discharge system, though of a much smaller scale. The electron beam is provided by an Energy Sciences Inc. Model CBP 175/5/15 Electrocurtain electron gun. The gun is a slightly modified version of one available and used in industry. It can be operated CW or pulsed up to 1000 Hz at energies up to 175 kV. It is a hot cathode, grid-controlled gun. Electrons are "boiled" off of a low work function cathode heated by a metal filament and guided into the accelerating region by a potential established across a metal grid structure. Once past the grid, the electrons are accelerated by the gun potential, up to 175 kV, and pass out of the gun to the discharge region via a metal foil window. The potential across the grid controls the current by determining how many electrons are accelerated. The gun potential determines the energy of the electrons. The window was a 0.5 mil titanium foil having dimensions of 5 cm by 17.5 cm.

The gun was operated at 175 kV to reduce loss in the foil and minimize foil heating, which is the primary cause of foil failure. Pulsing was accomplished at a rate of 5 Hz using 5 μ sec pulses. The rise time and fall time of the gun pulse were measured and found to be approximately 1 μ sec, which was believed to be short enough so as not to influence any of the measurements. Varying the grid potential provided a pre-foil current output range of 15-195 mA per pulse.

In actual practice, it was desirable to switch back and forth between pulsed and CW operation. However, to change from pulsed operation to CW required the opening of the high voltage storage tank and physical replacement of the pulsed grid circuit with the CW grid circuit. This exercise was very time-consuming. To facilitate matters, the pulsed circuitry was modified to accommodate either mode of operation, the choice being made by a remote switch. This circuit design proved satisfactory for pulsed operation, but yielded low CW currents and was marginal in this mode. As this was to be a pulsed experiment, the circuit was left intact. A problem arose, however, because of the above modification. The gun was normally brought up to operating conditions in the CW mode, then switched to pulsed. In preparation for shut-down, the gun was switched back to CW. It was found that great care must be exercised when switching modes while at operating conditions. Due to the high voltage power supply (2.5 kV) and large capacitors

used to drive the grid in the pulsed mode, the CW circuit, which is designed to accommodate less than 40 V, could be overloaded if the remote relays failed to activate simultaneously. The result can be, and was, in one instance, a catastrophic failure of the CW circuit to include burned and fractured resistors and diodes. Damage to the pulsed circuitry was also found. To preclude this event, it was necessary to turn off the power to the grid circuit prior to switching modes.

Discharge Chamber

The discharge chamber was stainless steel lined with quartz plates to insulate the high voltage electrode from the metal walls of the chamber. The anode was positioned just beneath the electron gun foil and consisted of a set of 1.6 mm diameter rods laid horizontally in the direction of gas flow. The anode was held at ground potential. The cathode was a polished stainless steel plate with rounded edges and had dimensions of 8.26 cm by 20.32 cm. A current button 2.57 cm in diameter and made of the same material was installed in the cathode but insulated from it by a 6 mm sleeve of dielectric. This button was centered in the short dimension, but offset 5.87 cm from the centroid of the cathode. While at the same potential as the electrode, the button was designed to provide discharge current readings that would be free from possible fringe effects that the entire electrode might experience. Mounted on a micrometer, the height of the cathode from the bottom of the chamber

could be varied. This allowed the electrode separation to be set anywhere from approximately 0.95 cm to 3.5 cm. Most experiments were run with a separation of 2.2 cm. The movable electrode eliminated the need for Langmuir probes for cathode fall measurements. Windows for viewing the discharge were located at both ends of the chamber and also downstream in the diffuser section.

The quartz plates are held in place by a substrate material similar to a very low vapor-pressure epoxy. Prolonged exposure to the heat and x-rays produced by the electron gun discolors this substrate and may cause it to break down. The latter case seems to have occurred during the course of early testing of the system. Upon application of voltage to the cathode, a sustained arcing was observed in the chamber. Upon removal of the chamber from the flow loop and removal of the cathode, it was found that the substrate had decomposed at one junction of plates providing a direct arc path to the grounded walls of the chamber. The gap was filled with quartz fragments and sealed with a new layer of substrate.

The flow loop and discharge chamber had been built for operation at pressures of 10^{-8} to 10^{-9} torr and had routinely been pumping into the low 10^{-7} torr range. Upon re-installation of the chamber with the new substrate, the system would pump down to no less than 1.2×10^{-5} torr. Figure 3 is a plot of pressure versus time recorded after the vacuum pumps had been valved off. The linearity of the

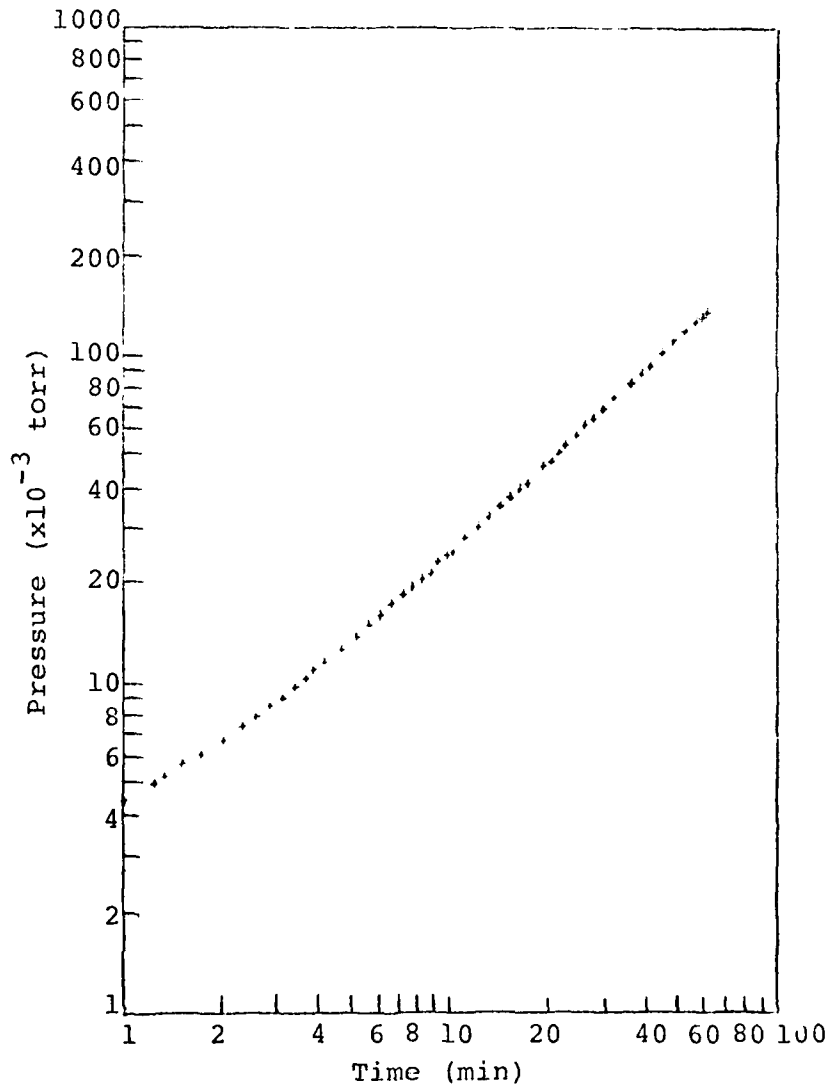


Fig 3. Flow Loop Leak Rate

curve clearly indicates that the leak is external. (If the problem were one of outgassing, the curve would tend to bend over as the vapor pressure of the material was reached. After that point the pressure in the chamber would have remained constant.) Using standard leak checking procedures, an apparent leak was found near one of the internal weld joints of the discharge chamber. The exact joint location was not determined. Time constraints precluded repair of the joint. While this situation allowed for the possibility of a greater effect on the experiment from external contaminants such as H₂O, the results should still be useful. Further, from Figure 2, the leak rate can be calculated to be approximately 2.2×10^{-3} torr/min starting at 1.2×10^{-5} torr. Since the experiments will be performed at or near atmospheric pressure, it was expected that the leak rate would be even less when the loop was filled with gas. After completion of this experiment, two leaks were actually found. One leak was in the button high-voltage feedthrough assembly. The second leak was found in the large bellows valve that was used to seal off the vacuum pump from the rest of the flow loop.

Voltage was supplied to bias the cathode negatively from a 30 kV power supply. The voltage drop was limited by a 1 μ f, 30 kV capacitor in parallel with the sustainer electrodes. The current was to be limited to some value above that drawn by the discharge but such that the chamber would

be protected in the event of an arc. The current limiter was a large pass-tube capable of holding off the 1 μ f capacitor. This circuit was to provide the capability of operating at high E/N values. However, it was found that the pass-tube was limiting the current to a value lower than the discharge current, thus creating enormous drops in the sustainer voltage. This situation was unacceptable and the above circuit was abandoned.

Since Meyer, et. al. and Douglas-Hamilton have shown that the most dramatic changes in the recombination occur at low values of E/N, it was decided that a smaller power supply could be used (Ref 14:88; 4:4822). A Spellman 5 kV current-limited supply replaced the larger supply. Again a 1 μ f, 30 kV capacitor was installed to stabilize the voltage. This circuit provided up to 5.2 kV with a maximum voltage drop of 5%, yielding an E/N range of up to approximately 9 Townsend for the 1/1.6/3, CO₂/He/N₂ gas mixture.

Closed-Cycle Flow Loop

The closed-cycle flow loop was constructed of 15 cm diameter high-vacuum, stainless steel ducts connected with Conflat flanges. Total volume of the loop was approximately 100 liters. The loop was equipped with a 1 kw heat exchanger for removal of waste heat generated by the discharge. Circulation of the gas was accomplished by an axial fan. The fan was externally driven with the drive mechanism sealed from the loop by a ferrofluidic rotary seal. Fan speeds of

up to 11,500 rpm were possible with this system. Only high purity gases were used, e.g., Grade 6-He, Grade 5-N₂, and Grade 4-CO₂. The gas inlet manifold used high-vacuum valves and ultrapure gas regulators.

The loop was evacuated via an ultrahigh-vacuum valve with a Leybold-Heraeus NT450 turbomolecular pump. After bakeout, the system could achieve pressures in the 10⁻⁸ torr range. This capability to form such a high vacuum allows unique opportunities to study the growth and effect of plasma chemical by-products with assurance that the contaminants are not coming from the atmosphere or the system components. The discharge chamber is connected to the loop via bellows ducting and flanges with knife-edge seals at both the inlet and outlet sections of the chamber. As noted above, the leak in the discharge chamber degraded to overall system vacuum performance to the low 10⁻⁵ torr range.

The closed-cycle flow loop described above was used with a previous device. More detailed information about the loop can be found in Reference 10.

Diagnostics and Data Reduction

Measurement of the recombination rate essentially involved monitoring the decay in the discharge current after the termination of external ionization from the electron gun. The discharge current through the current button was determined using a Pearson Pulse Transformer Model 411 with a sensitivity of 0.1 V/A. The transformer coil was positioned around the high voltage cable connecting the button to the

main electrode high voltage connection. A Pearson Model 110 coil having the same sensitivity as above was used on the high voltage line from the capacitor to the electrode. This second coil monitored all of the discharge current passing through the electrode and the button. The discharge voltage was measured using a high voltage probe. All three signals could be input to a Tektronix Model 7904 oscilloscope via standard coaxial cables and BNC connections. The Pearson coils had a rated accuracy of +1%. The high voltage probe was rated at $\pm 9\%$. The vertical display of the scope had a nominal accuracy of $\pm 2\%$.

The discharge current signal was to be sent to a Biomation Model 8100 Transient Recorder which would digitize the current decay curve. The digitizer provided up to 2024 storage locations and sampling intervals of 0.1 μsec to 10 sec. The resolution of the analog-to-digital converter was one part in 256 or 0.4%. Data stored by the digitizer would then be output via an internal digital-to-analog converter to a standard Y-T chart recorder. This curve was then to be digitized using a Hewlett-Packard Model 9845 computer and 9872A plotter. The computer would then fit Eq. (12) to the data using a nonlinear least-squares fit program available from Hewlett-Packard. A problem arose, however, that made the Biomation digitizer unusable. During testing it was found that even at the highest E/N values attainable with the Spellman power supply at an electrode separation of

2.2 cm, the current through the button was less than 100 mA. The resulting signal was thus only 10 mV and the minimum input scale on the digitizer was 50 mV. The low signal had great difficulty being properly processed by the digitizer.

As an alternative to the digitizer, it was decided to display the signal on the oscilloscope and photograph the trace. This trace could then be digitized by the computer. Again, the signal from the button was too small and an amplifier fast enough not to distort the signal was not available. It was decided to use the signal from the entire electrode as this was usually 10-20 times larger than that from the button and could be used without amplification. While the electrode signal might suffer from fringing effects of the electric field on the edges of the electrode, time constraints dictated that some measurements be made this way so as to obtain at least preliminary results. Further, Meyer, et. al., observed that the current from the entire electrode was usually proportional to the button current in their device, thus suggesting that fringing effects were small (Ref 14:82).

The process of digitizing a curve using the HP 9845 computer and 9872A plotter proved to be a highly accurate method of obtaining the data points for the curve fit. To test the process, a plot of Eq. (12) using representative values for α , β , and n_{e0} was made. When the same plot was digitized at 21 points whose values were already known from

the plotting calculation, the difference in values ranged from 0.02% to 3% on n_e and 0% to 3% on t . The average error was 0.71% for n_e values and 0.29% for t values.

The accuracy of the curve-fitting process was tested in a similar manner. Idealized data was produced using Eq. (12) and the following set of values for the parameters:

$$n_{eo} = 1.0 \times 10^{12} \quad (14)$$

$$\alpha = 1.0 \times 10^{-7} \quad (15)$$

$$\beta = 1.0 \times 10^4 \quad (\text{Ref 5:62,64})$$

The program used the method of least-squares to fit the curve to the data points and was commercially available (Ref 17). Table IV lists the actual and the calculated values for α and β for three cases.

TABLE IV
Nonlinear Curve Fit Results

Case	α	β	Time(sec)	Scatter
Actual	1.00×10^{-7}	1.00×10^4		
1	1.00×10^{-7}	9.99×10^3	1×10^{-5}	0%
2	1.18×10^{-7}	-5.6×10^3	1×10^{-5}	5%
3	1.06×10^{-7}	9.43×10^3	5×10^{-4}	5%

Case 1 is for data obtained directly from the use of Eq. (12) with the given constants and demonstrates the accuracy of the procedure. The second case uses the same data, except the data has been modified to include a random error of between +5% and -5% in the values for n_e , the electron number density. The second case more closely models a real experimental situation where some uncertainty and random error will exist in the measurements. The second case produced larger errors with respect to the actual values, as would be expected due to the induced random error. Still, for the recombination rate, the error is only 18%, which while not optimal, is not unacceptable.

A question immediately arises with respect to Case 2 about how the attachment rate could be so drastically different from the actual value. The problem stems from the conditions assumed and the time scale over which the data was taken. When the ionization is turned off, the dominant loss mechanism initially is recombination. At later times attachment becomes increasingly important. For the rates assumed, the electron number density decrease is not very rapid, and the time scale used, 1×10^{-5} sec, covers only the early stages of the decline where recombination is predominant. Thus, one would expect an accurate value for α to be calculated. To obtain a more accurate value for the attachment rate, data must be used that covers a much longer time so that the attachment process has a chance to produce a significant effect.

In Case 3 the data has been analyzed over a time 50 times longer than the previous cases. The values calculated for α and β are both more accurate. While this time scale proved adequate for this set of assumed rates, it may be inappropriate for situations where the rates may differ drastically. To deal with the more general case, a parameter that is independent of the rates must be found to indicate when "enough" time has elapsed to yield accurate values.

One possible parameter is the ratio of the initial (n_{eo}) and final (n_f) electron number densities. This ratio is independent of time, since the final number density can be chosen by the experimenter to be any point along the curve. Since the ratio is independent of time, it is likewise independent of the rates as required. The next question is what value the ratio must have before "enough" time has elapsed.

Table V shows the errors in α and β as a function of n_{eo}/n_f for the same rates used previously. From the table, it is shown that errors of less than 10% in both α and β can be obtained for a ratio near 500. While higher accuracy may be obtained using a higher ratio, values in excess of 1000 are extremely hard to measure.

TABLE V

Rate Errors vs Number Density Ratio

n_{e0}/n_f	α	β
6.55	11.0%	46.3%
36.6	8.07%	15.3%
465	6.22%	5.69%

V Results and Analysis

Figure 4 shows calculated current decay curves using Eq. (12) and a value for n_{e0} which is representative of this experiment. Where α and β are not labeled with the curve, the values used were 10^{-6} cm³/sec and 10^3 sec⁻¹, respectively. The effects of different recombination and attachment rates are quite dramatic. A recombination rate of 1×10^{-6} cm³/sec is typical of what was expected based upon Meyer, et. al. (Ref 14:85). The anticipated attachment rate was less than 1×10^3 sec⁻¹ (Ref 5:64).

Measurements in CO₂ Mix

The loop was filled with 830 torr of 1/1.6/3, CO₂/He/N₂ gas mixture which yielded a number density of one amagat at 25°C. The electrode separation was 2.2 ± 0.01 cm. Measurements were taken at five different voltages spanning the range of the power supply and at four different beam current settings spanning the range of the electron gun. Table VI lists the raw data. Note that the cases marked with an asterisk were run after all the other cases and were a repetition of the first cases taken. The time differential was approximately two hours and only a slight decline in the discharge current was observed. This indicates that there may have been some long-term plasma chemistry changes taking place but they were not having dramatic effects.

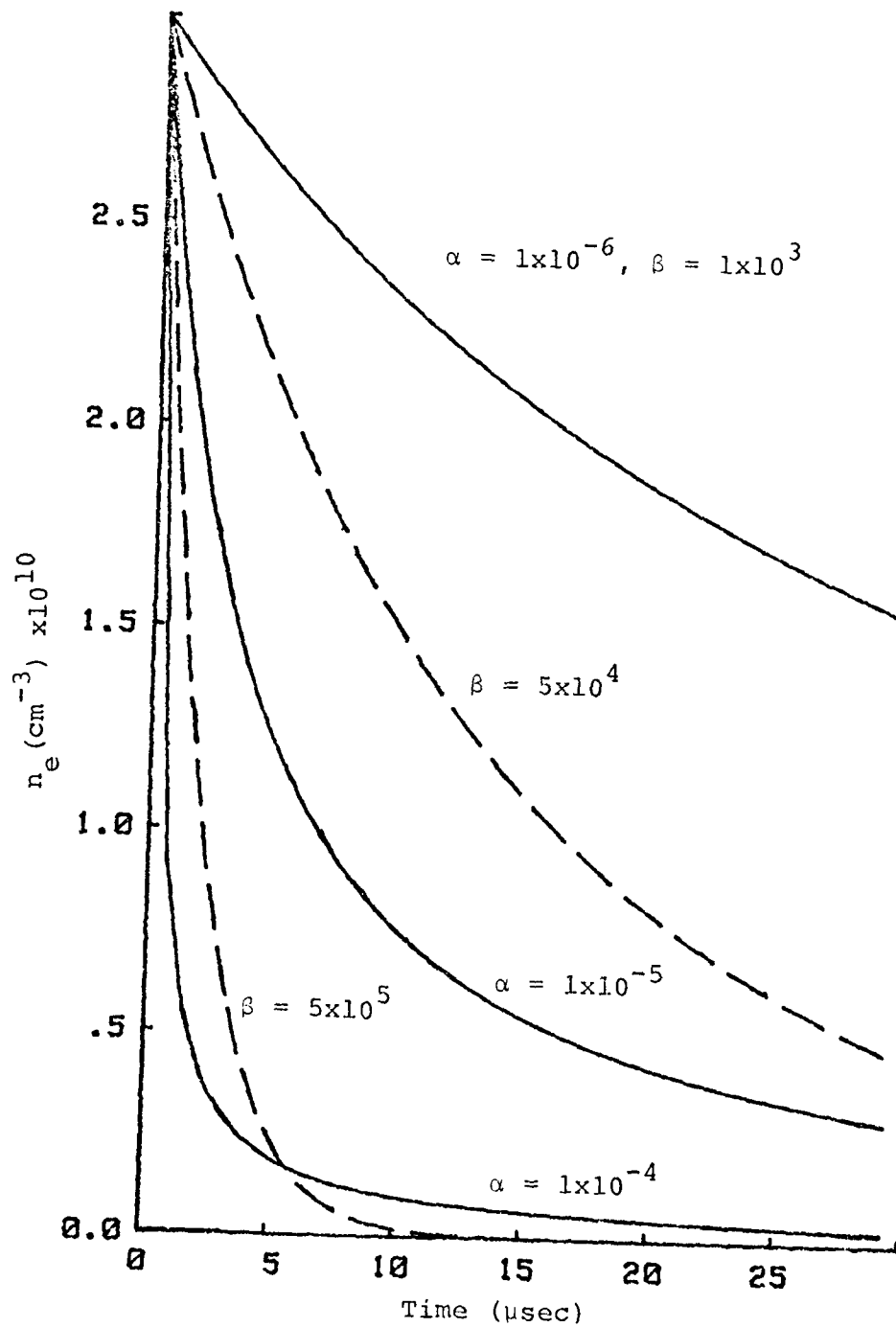


Fig 4. Calculated Current Decay Curves

TABLE VI

CO₂ Data

Case	1	2	3	4	5*	6	7	8	9	10*	11	12	13	14
Voltage (kV)	.6				→	1.8				→	2.94			→
Voltage Drop (V)	2	2	3	4	2	6	6	8	12	3	18	40	62	80
E/N (T)	1.01				→	3.04				→	4.97			→
Beam Current (mA)	55	99	148	195	55	55	99	148	195	55	55	99	148	195
Discharge Current (A)	.22	.315	.43	.55	.21	.46	.77	1.16	2.0	4.2	2.9	6.4	9.4	12.0
$n_{e0} \times 10^{10} \text{ (cm}^{-3}\text{)}$	1.17	1.68	2.29	2.93	1.12	.91	1.53	2.3	3.96	.832	4.08	9.0	13.2	16.9

Case	15*	16	17	18	19	20*	21	22	23	24	25*
Voltage (kV)	2.94	4.17				→	5.22				→
Voltage Drop (V)	18	60	105	140	180	60	110	160	200	270	110
E/N (T)	4.97	7.05				→	8.82				→
Beam Current (mA)	55	55	99	148	195	55	55	99	148	195	55
Discharge Current (A)	2.6	9.2	14.8	20.0	25.5	8.80	14.4	22.5	29.5	37.0	14.2
$n_{e0} \times 10^{10} \text{ (cm}^{-3}\text{)}$	3.65	10.8	17.3	23.4	29.9	10.3	14.3	22.3	29.3	36.7	14.1

Figure 5 is a reproduction of a typical discharge current trace. Note that the current has essentially dropped to zero by 12 μsec . This was typical of the CO_2 data. Some of the decay times were shorter, to approximately 8 μsec , few were longer than 12 μsec . These times were short with respect to those measured in N_2 discharges run by Douglas-Hamilton (Ref 4:4821).

The current decay curves were digitized and fits to the data were attempted using Eq. (12). While some of the plotted fits appeared accurate, all of the calculated recombination rates were obviously incorrect. Of 22 fits attempted, 17 gave values for α which were negative. The five positive values were in significant disagreement with values obtained by Meyer, et. al. in other $\text{CO}_2/\text{He}/\text{N}_2$ mixtures (Ref 14:85-87). Calculated attachment rates ranged from $3.9\text{-}9.3 \times 10^5 \text{ sec}^{-1}$. These values, while not unreasonable for the fast decay times observed, must be questioned because of the gross error in the recombination rates. Attempts to fit some of the data to a hyperbolic curve as Eq. (13) representing a recombination-dominated situation or an exponential curve representing an attachment-dominated situation were also unsuccessful.

Measurements in N_2

In light of the difficulty with the curve fitting process encountered above, it was decided to make a series of measurements in pure N_2 to determine if something in the

1/1.6/3, CO₂/He/N₂, 1 atm.

E/N = 8.82T, Beam Current = 148 mA

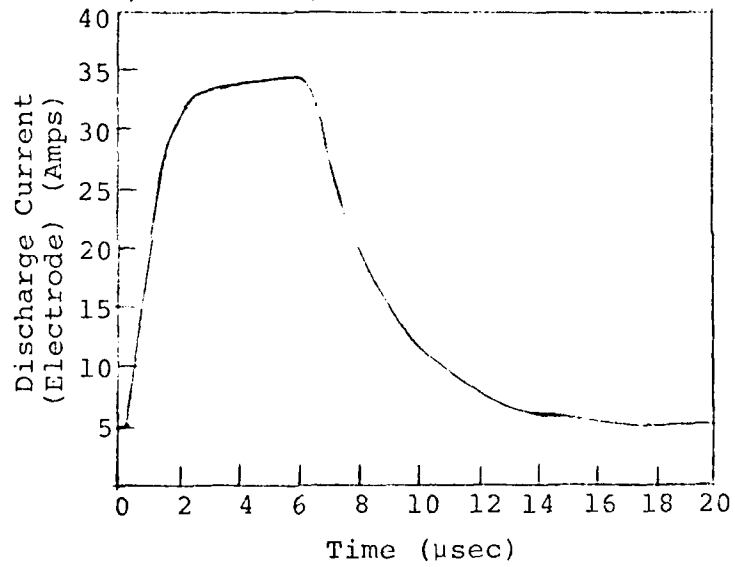


Fig 5. Discharge Current Pulse

procedure or equipment was at fault and also to attempt to baseline this system against published results (Ref 4). Table VII details the raw data. At low E/N, the decay times were approximately twice as long as those for CO₂. At measured E/N values of 4.97 Townsend on up, the decay time and total current grew significantly. Pulse lengths of 60-700 μ sec were required for the current to come to steady-state. Such pulse lengths resulted in large voltage drops. The decay times for the high E/N cases were hundreds of microseconds long. Since ideally there is no attachment in a pure N₂ discharge, it was expected that the decay times would be much longer than with CO₂.

Nonlinear fits to the N₂ curves were made using Eq. (12). Of the 10 attempts only three yielded rates somewhat in agreement, though not good agreement, with those of Douglas-Hamilton (Ref 4:4822). Table VIII lists the calculated rates for the three cases. The attachment rates are small, but not insignificant and are probably due to contaminants left over from the CO₂ mixture tests. It was noted that these were the cases requiring longer pulse lengths and having the very long decay times.

Data Modifications

The failure of the experimental procedure to yield reasonable results, except in a few cases, in both the CO₂ mix and N₂ indicated a fundamental problem with either the equipment or the data reduction method. An examination of

TABLE VII

N₂ Data

Case	1	2	3	4	5	6	7	8	9	10
Voltage (V)	600	→	→	1800	→	→	2940	→	→	4170
Voltage Drop (V)	3	10	5	4	10	10	5	350	460	700
E/N (T)	1.01	→	→	3.04	→	→	4.97	→	→	7.05
Beam Current (mA)	17	64	108	17	64	108	17	64	108	17
Discharge Current (A)	.078	.245	.390	.125	.450	.710	.16	4.0	13.4	2.95
n _{eo} x 10 ¹⁰ (cm ⁻³)	.72	2.28	3.63	.58	2.09	3.3	.596	14.9	49.9	6.46

TABLE VIII
Measured Rates in Nitrogen

F/N(T)	$\alpha \times 10^{-7}$ cm ³ /sec	Douglas- Hamilton	$\beta \times 10^4$ sec ⁻¹	Decay Time	Beam Current
4.97	5.53	1×10^{-7}	2.1	350 μ sec	64 mA
4.97	1.59	1×10^{-7}	4.4	250	108
7.05	9.48	8×10^{-8}	.17	1400	17

the experimental error due to the equipment or the digitizing process is discussed in the Appendix. The possible error from these sources clearly could not cause such drastic errors in the results.

A significant result arose in the process of testing the nonlinear fit program. Using data from one of the CO₂ curves, it was found that if the value of the electron number density of the first point, i.e., the value for n_{e0} at $t = 0$ on the decay curve, was changed, a better fit and much more reasonable rates were derived. This suggested that, in fact, the data analysis procedure did work, but that something was distorting the beginning of the decay curve. The pulse transformers and the oscilloscope had response times in the nanosecond range so these were ruled out as the sources of the problem. The discharge voltage was maintained across the electrodes at all times so there could be no response distortion. It was concluded that the

electron gun could not turn off fast enough to yield a proper decay curve. As noted previously, the fall-time of the gun was measured to be approximately 1 μ sec. For the low E/N N_2 cases and all of the CO_2 cases, the total decay time was 8-20 μ sec. Further, for the N_2 cases, the current had dropped to as low as 42% of the steady-state value in the first microsecond. It is clear that the previous assumption regarding the effect of the electron gun fall-time was in error and that, in fact, the gun does not turn off fast enough for these measurements. The N_2 cases in Table VIII had decay times so long that the electron gun fall-time was less significant and produced less distortion of the early part of the curve. An added complication arises from the fact that at the low E/N values used in this experiment, the power delivered by the electron beam was up to eight times the power in the discharge. Thus, when the gun is turned off, it is possible that significant changes can occur in the plasma conditions. If so, the electron kinetic rates would be time-dependent and the plasma after beam termination may bear little resemblance to the plasma during the pulse.

One possible solution to the problem might have been to begin the fit at a point greater than 1 μ sec from the start of the decay curve. While this could be done with only a slight modification to Eq. (12), it is doubtful that, for the data taken, an adequate ratio of initial to final

electron number densities could be obtained to yield a low uncertainty. For the CO₂ measurements, the current had dropped to typically 50% of the steady-state value within the first microsecond. Further, as noted previously, recombination is the dominant loss mechanism at early times, while attachment becomes dominant at later times. By eliminating so much of the curve, in terms of amplitude, the accuracy of the resulting recombination rate would be in serious question.

Steady-State Analysis

The rapid current decay times observed indicate large recombination and/or attachment rates. In the steady-state Eq. (10) defines the relationship between s and n_{eo} . Figure 6 shows calculated curves using Eq. (10) parameterized by different attachment rates. If the discharge was recombination-dominated, the plot would show a square root dependence of n_{eo} on s . If the discharge was attachment-dominated, the plot would be nearly linear. Figure 6 shows this effect quite well.

Figure 7 is a plot of the experimental data with linear least-squares fits performed on the results. (Two fits are made to the 3.04 T data. One uses all four data points but has a very poor correlation. The second fit uses only the first three points resulting in a very close correlation.) It appears that the discharge is, in fact, attachment-dominated. The attachment rates calculated from the

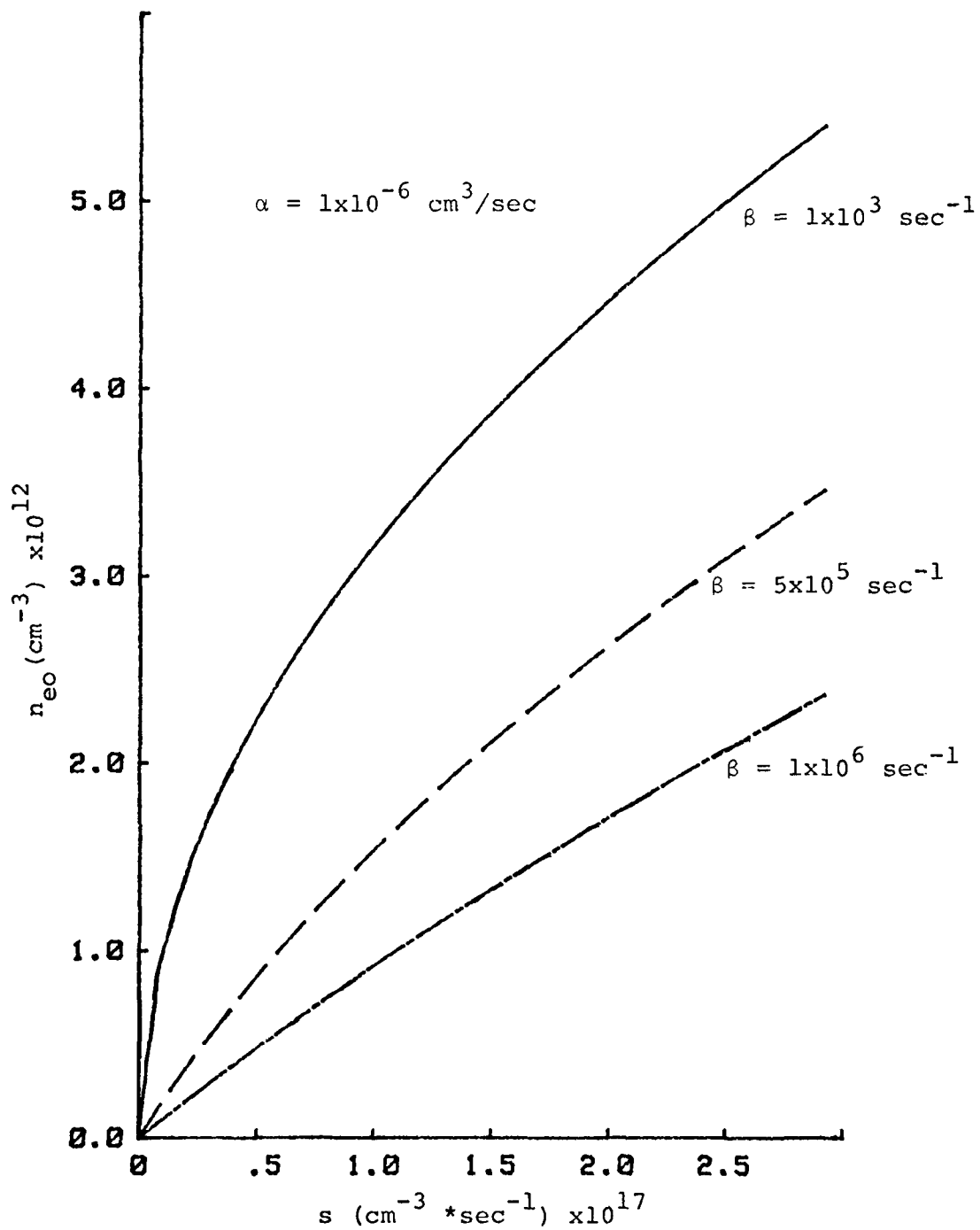


Fig 6. Calculated Electron Production Rate vs Steady-State Electron Number Density

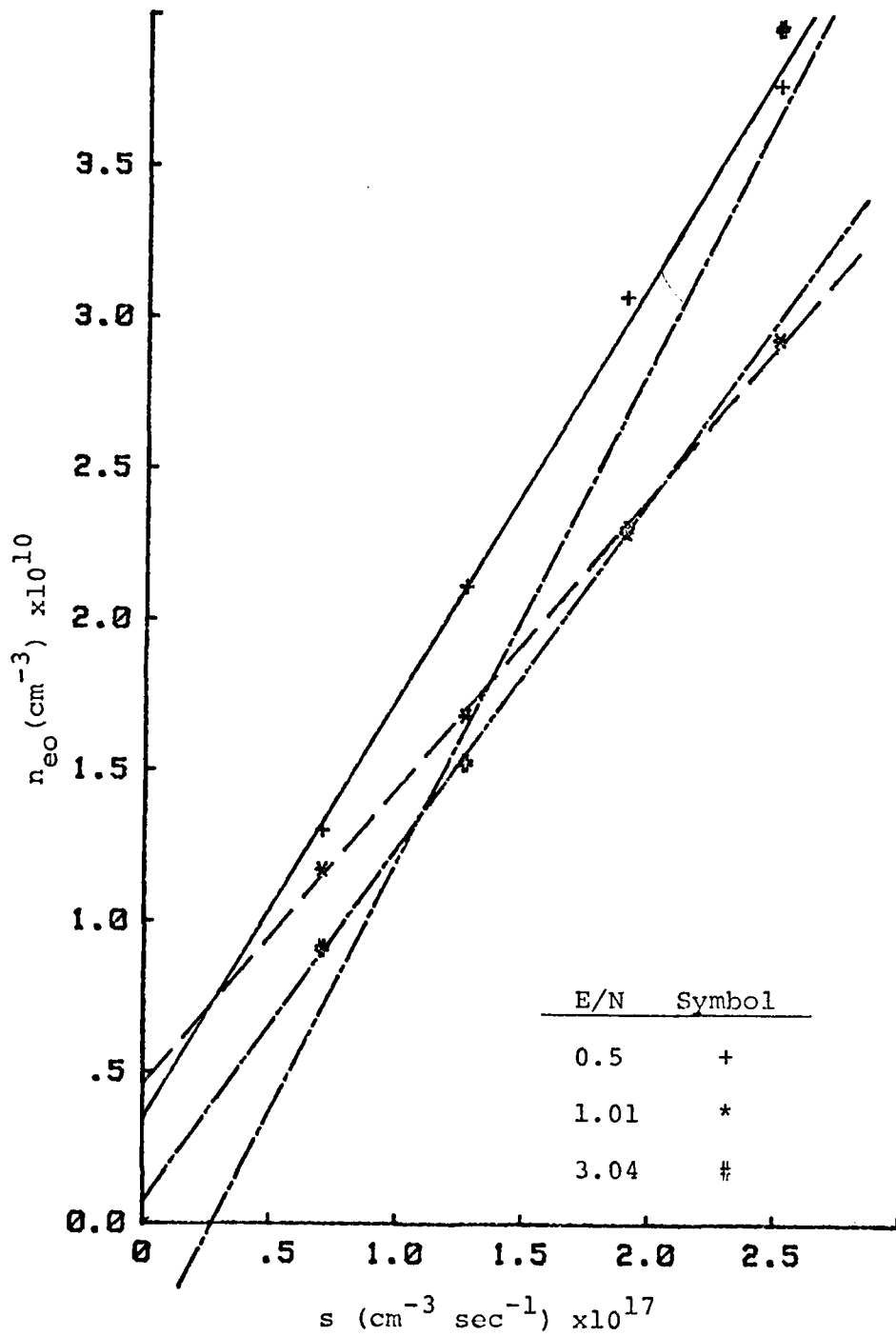


Fig 7. Electron Production Rate vs Number Density

slopes of the curves range from $0.6-7 \times 10^7 \text{ sec}^{-1}$, which are much larger than expected. In comparison with the curves in Figure 6, such large attachment rates could easily mask the expected recombination rate of $10^{-6} \text{ cm}^3/\text{sec}$.

It should be noted that these results do not include a correction for cathode fall (see Appendix). At these low voltages, the effect of cathode fall might reduce the E/N markedly. Such a reduction would yield a decrease in the drift velocity and a resulting increase in the calculated electron number density. However, at a given E/N, the overall effect would be to translate the curve up along the n_{e0} axis with no real change in the slope. The cathode fall data suggests the possibility of a decrease in the fall voltage as s increases. Such a circumstance could cause the curves in Figure 7 to arc over indicating a weaker attachment dominance. However, the cathode fall data is not complete enough for a thorough analysis.

Assuming the discharge is attachment-dominated, what is the source of the attachment? The likely species are CO_2 , O_2 , and H_2 , with the latter appearing as a contaminant from water vapor in the vacuum leak or the gas bottles. The oxygen could arise from the leak, gas bottles, or dissociation of CO_2 in the discharge. If one considers the process of dissociative attachment for these species, one finds that the threshold energies for the reactions are much greater than the average energy of the discharge electrons which is

approximately 0.5 eV or less. This is true even for vibrationally excited hydrogen.

A second possibility is that the electron beam electrons are the ones being attached. While these electrons have the necessary energy to access the cross-sections, at the highest beam current, there are only about 10^5 cm^{-3} compared to 10^{10} cm^{-3} in the discharge. Thus, even if all of the primary electrons were attached, because they are such a small fraction of the total number available, the effect would be minimal.

The third possibility is that a three-body attachment process with O_2 is occurring. This reaction occurs for thermal electrons and, thus, the low energy discharge electrons could access the cross-section. Using the rates for thermal electrons with the third body being either CO_2 , N_2 , or He, and assuming an attachment rate of $6 \times 10^6 \text{ sec}^{-1}$, a lower bound on the amount of O_2 needed can be found to be approximately $3.4 \times 10^{17} \text{ cm}^{-3}$ or 1.3% of the available gas. From the leak, at most 1×10^{-3} torr or about $3 \times 10^{16} \text{ cm}^{-3}$ are available. From contamination in the gas bottles, another 0.3% or $8 \times 10^{16} \text{ cm}^{-3}$ might be available. The amount created within the plasma is unknown. However, it appears that there might be enough O_2 from all of these sources to make this explanation plausible. Still, it must be understood that the actual rates for the slightly more energetic electrons in the discharge would be lower than the thermal electron rates used above.

VI Conclusions and Recommendations

Electron beam-sustained discharges were operated in a closed-cycle flow loop in a mixture of 1/1.6/3, CO₂/He/N₂ over a variety of beam currents and an E/N range of 0.5-9 Townsend. Steady-state analysis of the discharge current indicates that the plasma is attachment-dominated. Calculated attachment rates were $0.6-7 \times 10^7 \text{ sec}^{-1}$. Attempts to fit an analytic solution of the electron lifetime equation to the current decay curve were inconclusive due to distortion of the curve by the slow fall-time of the gun relative to the discharge current decay time. However, the curve-fit method was validated by fitting current decay curves for discharges in N₂ with good success. Plasma degradation due to plasma chemistry was not seen as significant for the conditions and time scale over which this experiment was operated.

The results of this study suggest a possible problem for laser plasma operation at low E/N values. The attachment rates determined above are large enough to possibly lead to attachment instabilities in the discharge, though none were observed here. However, the optimum E/N range for CO₂ laser operation is in the 20-30 T range, well above where these tests were made. It cannot be assumed that the same relative magnitudes of the electron loss processes will exist at these higher E/N values.

It is recommended that the 30 kV power supply circuit be modified so that it can be used to allow measurements at higher E/N values. Operation at higher E/N values may result in the discharge current decay times becoming much longer as in the case of N₂. If longer decay times do result, the distortion by the electron gun would be reduced. It is also suggested that an amplifier be found so that the current button and high-speed digitizer can be used. Further, if some sort of data interface could be developed to extract the stored data in its digital form from the digitizer and fed directly into the computer, errors from the intermediate digital-to-analog-to-digital conversion could be eliminated and data reduction turnaround improved.

Bibliography

1. Bevington, P. R. Data Reduction and Error Analysis for the Physical Sciences. New York: McGraw-Hill Book Co., 1969.
2. Bletzing, P. et al. "Influence of Contaminants on the CO₂ Electric-Discharge Laser," IEEE Journal of Quantum Electronics, QE-11:317-323 (7 July 1975).
3. Dettmer, J. W. Discharge Processes in the Oxygen Plasma. Wright-Patterson AFB, Ohio: Air Force Institute of Technology, 1978.
4. Douglas-Hamilton, D. H. "Recombination Rate Measurements in Nitrogen," Journal of Chemical Physics, 58: 4820-4823 (June 1973).
5. Douglas-Hamilton, D. H. and R. S. Lowder. Carbon Dioxide Electric Discharge Laser Kinetics Handbook. AFWL-TR-74-216. Kirtland AFB, New Mexico: Air Force Weapons Laboratory, April 1975 (AD-A008 650/4GI).
6. Dzimianski, J. W. and L. E. Kline. High Voltage Switch Using Externally Ionized Plasmas. AFWAL-TR-80-2041. Wright-Patterson AFB, Ohio: Aero Propulsion Laboratory, April 1980.
7. Eckbreth, A. C. and P. R. Blaszk. "Closed-Cycle CO₂ Laser Discharge Investigations," Paper for AIAA 5th Fluid and Plasma Dynamics Conference. Boston, Mass.: June 1972.
8. Fenstermacher, C. A. et al. "Electron-Beam-Controlled Electrical Discharge as a Method of Pumping Large Volumes of CO₂ Laser Media at High Pressures," Applied Physics Letters, 20:56-60 (15 January 1972).
9. Garscadden, A. Private Communication (September 1980).
10. Grosjean, D. F. and R. A. Olson. Closed-Cycle Rare-Gas Electrical-Discharge Laser. AFAPL-TR-77-13. Wright-Patterson AFB, Ohio: Air Force Aero Propulsion Laboratory, April 1977.
11. Hasted, J. B. Physics of Atomic Collisions. London: Butterworth and Co., 1964.
12. Kasner, W. H. and M. A. Biondi. "Electron-Ion Recombination in Nitrogen," The Physical Review, 137:A317-A329 (18 January 1965).

13. Kast, S. J. and C. Cason. "Performance Comparison of Pulsed Discharge and E-Beam Controlled CO₂ Lasers," Journal of Applied Physics, 44:1631-1637 (4 April 1973).
14. Meyer, T. W. et al. "Electron-Ion Recombination Rates in Laser Gas Mixes," Laser Digest. AFWL-TR-77-15. Kirtland AFB, New Mexico: Air Force Weapons Laboratory, pp 80-90, March 1977.
15. Phelps, A. V. and R. D. Hake. "Momentum-Transfer and Inelastic-Collision Cross Sections for Electrons in O₂, CO, and CO₂," Physical Review, 158:70-84 (5 June 1967).
16. Reilly, J. P. "Pulsed/Sustainer Electric-Discharge Laser," Journal of Applied Physics, 43:3411-3416 (August 1972).
17. System 45 Software: Non-Linear Regression Analysis. Loveland, Colorado: Hewlett-Packard Inc.
18. Tannen, P. D. et al. "Species Composition in the CO₂ Discharge Laser," IEEE Journal of Quantum Electronics, QE-10:6-11 (January 1974).
19. Thoenes, J. and S. C. Kurzius. EDL Performance Model: Part III - Analysis of Closed Cycle Electron-Beam Sustained CO₂ EDL with Air Contaminant. Technical Report RG-CR-75-2. Redstone Arsenal, Alabama: Army High Energy Laser Directorate, May 1976.
20. Von Engel, A. Ionized Gases (Second Edition). London: Oxford University Press, 1965.
21. Wiegand, W. J. and W. L. Nighan. "Plasma Chemistry of CO₂-N₂-He Discharges," Applied Physics Letters, 22: 583-586 (1 June 1973).

Appendix

Error Analysis

Cathode Fall

The most significant source of error in the measurements was accounting for the cathode fall potential which is typically a few hundred volts. An attempt to determine the cathode fall voltage was made by establishing a current at a particular combination of voltage and electrode separation, then varying the separation and voltage while maintaining that constant current. The procedure is similar to using probes except the probe in this case is the electrode and a constant E/N is maintained by keeping the current constant. Measurements were made at three different E/N values, three different electron gun currents, and five different electrode separations. Since the cathode fall is primarily dependent on the electrode material and gas mixture, the different E/N curves should all intersect at the zero-separation point at or near the same voltage value. After performing linear fits of the data, it was found that disparities of up to several hundreds of volts existed between the intercept values. It was noted that at two of the three E/N values the fall voltage showed a decline with increasing beam current. Time constraints prevented accumulation of enough data to further examine this trend and to resolve the disparities in the calculated fall voltages. Thus, none of the results in this report account for the cathode fall voltage.

Equipment Error

Using standard error propagation analysis techniques, it can be shown that the values for E/N , n_e , α , and β can be found with good precision (Ref 1:64). Table IX is a summary of the rated or worst case accuracies of the equipment and signal values.

TABLE IX
Equipment and Signal Accuracies

Electrode Area	-- ±1%
Pulse Transformer	-- ±1%
Oscilloscope	-- ±2%
Voltage Probe	-- ±9%
Pressure	-- ±1%
Drift Velocity	-- ±5%
Voltage	-- ±5%
Current	-- ±3%

The large error in the voltage results from the worst case voltage drop during the discharge. Most voltage drops were 3% or less and the voltage on the scope could be read in the worst case to ±3%. The uncertainty in the voltage, electrode area, and pressure yield a worst case uncertainty in the value of E/N of 5.6% exclusive of cathode fall. If the worst case for the uncertainty in the drift velocity is assumed to be the addition of the 5% calculated error and the 5.6% error from the value of E/N , the resulting error

in the drift velocity is 10.6%. This is the primary uncertainty in the electron number density. Evaluating Eq. (6) with the above uncertainties, the precision of the value of n_e is found to be 12%.

It is not possible to predict precisely what the uncertainty in α and β will be as a result of the curve-fitting process. The program does calculate confidence intervals which can be used to bound the values. With respect to the analysis performed based on the ratio of the initial to the final electron densities, a crude error estimate can be made. Upon reviewing the data, the ratio of initial to final electron density was typically around 100. Based on the previous analysis, the uncertainty on α and β could thus be inferred as being approximately 10%. A more detailed case-by-case estimate would be required to assign a smaller value.

VITA

Greg R. Schneider was born on 13 December 1953 in Davenport, Iowa. He graduated from high school in Rock Island, Illinois in 1972 and attended the United States Air Force Academy from which he received the degree of Bachelor of Science in Physics in June 1976. Upon graduation he received a Regular commission in the USAF. He was assigned to the Advanced Laser Division of the Air Force Weapons Laboratory at Kirtland AFB, New Mexico from June 1976 until entering the School of Engineering, Air Force Institute of Technology, in June 1979.

Permanent address: 2432-19 Avenue
Rock Island, Illinois 61201

1-1 REPORT DOCUMENTATION PAGE		READ INSTRUCTIONS BEFORE COMPLETING FORM
1. REPORT NUMBER AFIT/GER/PH/80D-8	2. GOVT ACCESSION NO. AD A094398	3. RECIPIENT'S CATALOG NUMBER
4. TITLE (and Subtitle) INVESTIGATION OF ELECTRON LOSS PROCESSES IN CO ₂ /He/N ₂ ELECTRIC DISCHARGES.		5. TYPE OF REPORT & PERIOD COVERED M.S. Thesis
7. AUTHOR(s) Greg R. Schneider Capt, USAF		6. PERFORMING ORG. REPORT NUMBER
9. PERFORMING ORGANIZATION NAME AND ADDRESS Air Force Institute of Technology (AFIT-EN) Wright-Patterson AFB, Ohio 45433		8. CONTRACT OR GRANT NUMBERS
11. CONTROLLING OFFICE NAME AND ADDRESS		10. PROGRAM ELEMENT, PROJECT, TASK AREA & WORK UNIT NUMBERS
14. MONITORING AGENCY NAME & ADDRESS (if different from Controlling Office) (12) 73		12. REPORT DATE December 1980
		13. NUMBER OF PAGES 73
		15. SECURITY CLASS. (of this report) Unclassified
		15a. DECLASSIFICATION/DOWNGRADING SCHEDULE
16. DISTRIBUTION STATEMENT (of this Report) Approved for Public Release; Distribution Unlimited.		
17. DISTRIBUTION STATEMENT (of the abstract entered in Block 20, if different from Report) Approved for Public Release; IAW AFR 190-17 06 JAN 1981 FREDERICK C. LYNCH, Major, USAF Director of Public Affairs		
18. SUPPLEMENTARY NOTES		
19. KEY WORDS (Continue on reverse side if necessary and identify by block number) Electron Beam-Sustained Discharge CO ₂ Electric Discharges Closed-Cycle Discharge Electron-Ion Recombination Electron Loss Processes Electron-Neutral Attachment		
20. ABSTRACT (Continue on reverse side if necessary and identify by block number) An investigation of electron loss processes in electron beam-sustained discharges of an atmospheric pressure gas mixture of 1/1.6/3, CO ₂ /He/N ₂ in a closed-cycle flow loop was conducted. Steady-state analysis of the discharge current indicates that the discharge is dominated by electron-neutral attachment at rates of approximately 10 ⁶ sec ⁻¹ in the E/N range of 0.5-9 Townsend. Attempts to fit an analytic solution of the electron lifetime equation to the discharge current decay curves were inconclusive due to the slow fall-time of the electron gun relative to the current decay time. Changes in the discharge		

20. Abstract (Continued)

characteristics due to chemical reactions in the plasma were not significant.

2

DATE
FILME